Role of interspecies interactions in the preparation of a low-entropy gas of polar molecules in a lattice

A. Safavi-Naini, M. L. Wall, and A. M. Rey

Phys. Rev. A **92**, 063416 — Published 18 December 2015

DOI: 10.1103/PhysRevA.92.063416

The Role of Interspecies Interactions in the Preparation of a Low-entropy Gas of Polar Molecules in a Lattice

A. Safavi-Naini,[1] M. L. Wall,[1] and A. M. Rey[1]

[1] *JILA, NIST and Department of Physics, University of Colorado, 440 UCB, Boulder, Colorado 80309, USA*

The preparation of a quantum degenerate gas of heteronuclear molecules has been an outstanding challenge. We use path integral Quantum Monte Carlo simulations to understand the role of interactions and finite temperature effects in the protocol currently employed to adiabatically prepare a low-entropy gas of polar molecules in a lattice starting from an ultracold Bose-Fermi mixture. We find that interspecies interactions affect the final temperature of the mixture after the adiabatic loading procedure and detrimentally limit the molecular peak filling. Our conclusions are in agreement with recent experimental measurements [1] and therefore are of immediate relevance for the myriad experiments that aim to form molecules from dual-species atomic gases.

I. INTRODUCTION

Polar molecules, interacting via long-range and anisotropic dipolar interactions, hold great promise as quantum simulators hosting exotic quantum phases [2, 3], as well as a diverse range of phenomena, ranging from quantum magnetism [4], to many-body localization [5], to synthetic spin-orbit coupling [6, 7]. A necessary ingredient for simulating these these behaviors is to the ability to reach low entropy conditions. However, despite the rapid experimental progress, a reliable method to form such a state has remained out of reach [8–10]. The two main obstacles to realizing a low-entropy state are the inapplicability of standard atomic cooling techniques to polar molecules and the requirement to suppress chemical reactions. A proposed solution to these problems is to form the molecules directly in a deep optical lattice through association after optimally loading a degenerate atomic gas mixture [11–18, 27, 28]. This protocol is shown schematically in Fig. 1. However, in order for this scheme to be a reliable pathway, it is necessary to have a high atom/molecule conversion efficiency. While there are many steps in converting the atomic mixture to a molecular gas which can degrade the efficiency of molecule production, the main bottleneck is creating a large region where the densities of the two atomic species overlap and correspond to exactly one atom of each species per lattice site. Temperature, interactions, and loading conditions can significantly limit the achievement of this requirement.

Here, we use path integral Monte Carlo simulations (QMC) based on the worm algorithm [29], as well as its two-worm extension, to investigate the effects of finite temperature and interspecies interactions during adiabatic loading from a dipole trap into an optical lattice. We show that the final temperature of the lattice system following adiabatic loading depends strongly on the strength and sign of interspecies interactions, and can be far from the ideal, zero-temperature regime. In contrast to previous studies, which do not treat the adiabatic loading procedure and find that attractive interspecies interactions enhance the on-site densities [30, 31], our analysis predicts that both attractive and repulsive

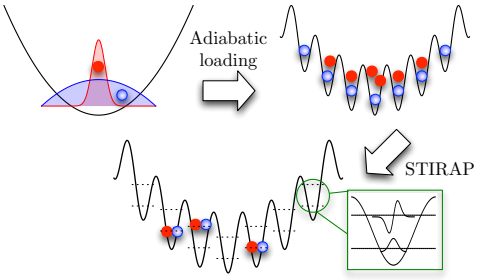

FIG. 1. (Color online) *Production of ground state molecules from a dual-species mixture.* (Top line) A finite-temperature dual-species gas of bosonic species A atoms (red) and fermionic species B atoms (blue), is adiabatically loaded from a harmonic trap into an optical lattice in the presence of interspecies interactions. The initial temperature and interactions determine the temperature, density overlap, and peak filling of the mixture. (Bottom line) Following STIRAP, only those sites with exactly one atom of each species are converted to a ground state molecule, with some probability to excite the molecule to a higher lattice band (schematic wavefunctions in green box).

interactions can lead to substantial depletion of on-site densities of the bosonic species and takes into account the contributions of dimensionality, effective mass imbalance, and quantum statistics [32–34]. We also discuss the efficiency of magnetoassociation, in which two atoms on the same site are converted into a weakly bound Feshbach molecule, focusing on the role of motional excitations and the difference between harmonic oscillator and lattice-based treatments. Finally, we discuss the impact of imperfections in stimulated Raman Adiabatic Passage (STIRAP), which is used to convert Feshbach molecules to ground state molecules, on the ground state molecule production [11, 35]. We study the adiabaticity of this protocol, and provide approximate analytical formulas which can be used to determine the probability of promotion of molecules to higher bands during the STIRAP procedure. Since molecules in higher bands have a much larger tunneling rate, an appreciable higher band population can greatly impact dynamics involving molecular motion. We find that for experimentally relevant param-

eters there is no significant population transfer, provided the Lamb-Dicke criterion is satisfied. Our conclusions are corroborated by the recent experimental observations reported in [1] and thus of fundamental importance for ongoing experimental efforts to achieve a high-filling lattice gas of ground state polar molecules.

II. SINGLE-COMPONENT GASES IN THE LATTICE

We begin by studying trapped single-species gases of bosons or fermions. We assume the bosons are trapped in a deep lattice where they can be described by the Bose-Hubbard Hamiltonian with an additional external harmonic confinement:

$$H = -\sum_{\langle i\,j\rangle} J_{\rm A}(a^\dagger_{i,{\rm A}}a_{j,{\rm A}} + {\rm h.c.}) + \frac{U}{2}\sum_i n_{i,{\rm A}}(n_{i,{\rm A}}-1) - \sum_i \mu_{i,{\rm A}} n_{i,{\rm A}}. \quad (1)$$

Here, $a^\dagger_{i,{\rm A}}$ ($a_{i,{\rm A}}$) is the bosonic creation (annihilation) operator for species "A" and $n_{i,{\rm A}} = a^\dagger_{i,{\rm A}}a_{i,{\rm A}}$. The first and second terms in the Hamiltonian Eq. (1) are the tunneling $J_{\rm A}$ and the on-site interaction, assumed repulsive with strength $U > 0$, respectively. Finally, $\mu_{i,{\rm A}} = \mu - \sum_{\xi=x,y,z} w_\xi \xi_i^2$, where w_ξ and ξ_i are the strength of harmonic confinement and the coordinate of site i along axis ξ, respectively, and μ is the chemical potential.

In order to facilitate comparisons with the experimental data in [1], we will use ^{87}Rb for species A, but we stress that our conclusions apply for generic bosonic species described by the Bose-Hubbard model. The effective external harmonic confinement includes the additional confinement due to the curvature of the lattice beams. The A atoms are assumed to experience a lattice potential $V_0 = 20E_A$, where E_A is the recoil energy of the A atoms.

To characterize the density as a function of atom number, we first match the entropy of the gas in the dipole trap to the one in the lattice and find the final temperature $T_{\rm fin}/J_{\rm A}$. The bottom right inset of Fig. 2 shows an example of this procedure for 3000 atoms. The solid green line shows the entropy of a weakly interacting Bose gas, which describes the A atoms in the harmonic trap. Blue triangles denote the entropy of the A atoms after loading into the lattice, given by

$$S_f(T) = \frac{E(T)-E(0)}{T} + \int_0^T \frac{E(T)-E(0)}{T^2}\,dT, \quad (2)$$

where $E(T)$ is the system energy at temperature T. Both $E(T)$ and $E(0)$ are directly measured in our QMC simulations. An example of the entropy matching procedure for an initial temperature $T_i = 0.4T_c$, T_c the critical temperature for Bose-Einstein condensation, is shown with dashed arrows.

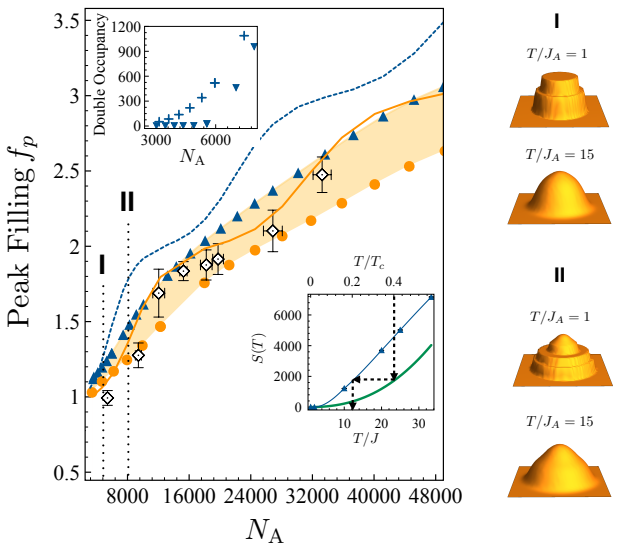

FIG. 2. (Color online) *Peak filling of* species A vs. atom number. (Main panel) The peak filling f_p as a function of number of ^{87}Rb atoms at $T/J_{\rm A} = 15$, used as an example of bosonic species A, with a lattice depth of $V_0 = 20E_{\rm A}$ given for harmonic confinements of $\omega_r\,(\omega_z) = 2\pi\times 40(260)$ Hz (filled triangles) and $2\pi\times 35(227)$ Hz (filled circles). Empty diamonds are experimental data [1]. The dashed (solid) line shows the on-site density at the center of the trap at $T/J_{\rm A} = 15$ for the weaker (stronger) harmonic confinement. (Lower inset) Entropy matching procedure for ^{87}Rb following adiabatic lattice loading with strong harmonic confinement. Solid green line is weakly interacting gas and blue triangles are ∼3000 lattice-confined Rb. (Upper inset) Double occupancy at $T/J_{\rm A} = 1$ (filled upside-down triangles) and $T/J_{\rm A} = 15$ (crosses) for the strong harmonic confinement. (Right panels) Integrated density $n(x,y)$ at points marked I and II at $T/J_{\rm A} = 1$ (upper) and $T/J_{\rm A} = 15$ (lower) for strong harmonic confinement.

Next we determine the peak filling, f_p. To compare with the experimental procedure of extracting the peak filling, we first integrate along z and mimic the experimental imaging resolution by applying a Gaussian filter with a width of 4 sites to the integrated density. We fit the resulting density to a Thomas-Fermi (TF) distribution $n(x,y) = \frac{4}{3} f_p \sigma_z \left[1-(x/\sigma_x)^2-(y/\sigma_y)^2\right]^{3/2}$. The extracted f_p values are plotted in Fig. 2 as a function of atom number, $N_{\rm A}$, after the adiabatic loading procedure, with filled circles (triangles) for two different trapping conditions. The filling at the center of the trap is displayed with dashed (solid) lines for the weaker (stronger) harmonic confinement at $T/J_{\rm A} = 15$. The empty diamonds are the experimental results [1]. The rightmost panels of Fig. 2 give examples of the resulting distributions integrated along the z-axis, $n(x,y)$, for $N_{\rm A} \sim 4000$ (labeled I) and $N_{\rm A} \sim 8000$ (labeled II). For these two values of $N_{\rm A}$ we show the distribution at $T/J_{\rm A} = 1$ (top), which is the low-temperature result, followed by the in-

tegrated density distribution at $T/J_{\rm A} = 15$ (bottom), which is closer to the experimental temperature.

It is worth noting that while the density at the center of the trap is strongly dependent on temperature, f_p does not display a strong dependence on $T/J_{\rm A}$ within the experimentally-relevant temperature range. This is due to the process by which we obtain f_p, which includes integrating over one direction and fitting the resulting distribution to the TF distribution. These two steps wash out the features distinguishing the distributions at different temperatures. However, this does not mean that the efficiency of the formation of molecules is unaffected by temperature. This is evident if one probes the number of doubly occupied sites with increasing temperature. Sites with double (or higher) occupancies do not result in molecule formation. The upper inset of Fig. 2 shows the double occupancy at $T/J_{\rm A} = 1$ (inverted triangles) and $T/J_{\rm A} = 15$ (crosses). In the low-temperature regime ($T/J_{\rm A} = 1$) the first Mott shell extends to $N_{\rm A} \approx 5000$ particles, after which a superfluid region forms at the center of the trap, before transitioning to the second Mott shell at $N_{\rm A} \approx 8000$ (see the dashed blue line in Fig 2). However close to or above $T/J_{\rm A} = 15$, $5-10\%$ of the A atoms are in doubly occupied sites and hence will not participate in molecule formation.

Next, we consider the fermionic species B of the mixture, taking ^{40}K for comparison with recent experimental data [1]. However, as before, our conclusions are valid for generic fermionic species that can be described by a tight-binding model. The difference in the polarizability with respect to ^{87}Rb means that the ^{40}K atoms feel a lattice potential of depth $V_0 = 9E_{\rm B}$, where $E_{\rm B}$ is the B species recoil energy. At low temperatures, p-wave interactions in the spin-polarized gas can be neglected, and the determination of the density reduces to a non-interacting problem. As the harmonic trap is separable, this problem can be straightforwardly treated by direct diagonalization for the single-particle eigenenergies E_{n_ξ} and corresponding wavefunctions $|\psi_{n_\xi}\rangle$. With these single-particle quantities we can evaluate the grand canonical partition function, from which we find the entropy per particle S/N, as well as the on-site density,

$$n(\xi) = \textstyle\sum_{n_\xi} \frac{1}{1+\exp(\beta(E_{n_\xi}-\mu))} |\psi_{n_\xi}(\xi)|^2 \,, \qquad (3)$$

where $\xi = \{x, y, z\}$ and $\beta = 1/T$ is the inverse temperature.

In Fig. 3 we show the peak filling of species B as a function of atom number. For fermions we use a Gaussian fit with $n(x,y) = \sqrt{2\pi\sigma_z} f_p \exp\left[-x^2/(2\sigma_x^2) - y^2/(2\sigma_y^2)\right]$ after integration along z. Here, we also account for the experimental imaging resolution and pixelation by applying a Gaussian filter. The band, delimited by the blue triangles and orange squares, shows the range of peak fillings for $1 < T_{\rm fin}/J_{\rm B} < 5$, with $J_{\rm B}$ the tunneling of the B atoms. As the temperature of the B atoms in the lattice increases, so does the width of the cloud, resulting in a decrease in the peak filling. The empty diamonds show the experimental data [1]. The plateau indicates the atoms forming an incompressible band insulator. On the right panel we show the integrated density distribution at points marked I and II. At II, the B atoms form a band insulator in a large region of the lattice.

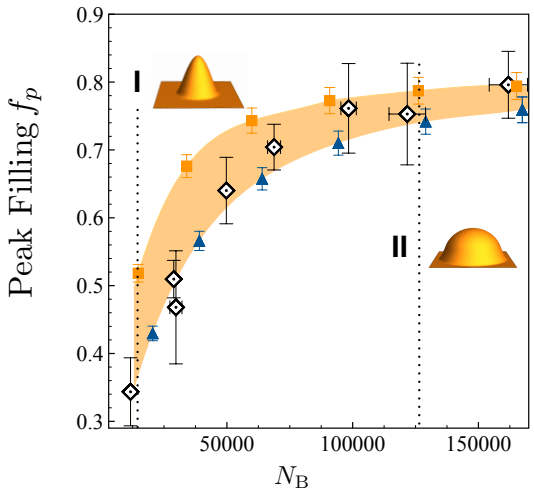

FIG. 3. (Color online) *Peak filling of the fermionic species B vs. atom number.* (Main panel) The peak filling of ^{40}K, used as an example for the fermionic species B, at $T_{\rm fin}/J_{\rm B} = 1$ (filled squares) and $T_{\rm fin}/J_{\rm B} = 5$ (filled triangles) extracted from the integrated density distributions $n(x,y)$, including mimicked resolution and pixelation effects. Results are for harmonic trap frequencies $(40 \times 40 \times 260)$ Hz and a $9E_{\rm B}$ deep lattice. Empty diamonds show experimental results [1]. Insets show the integrated density distributions at points I and II .

III. LATTICE-CONFINED TWO-SPECIES MIXTURE

We use a two-component mixture of soft-core ("A") and hard-core ("B") bosons to study the combined effect of interspecies interactions and finite temperature on the density of the A species. Hard-core bosons act as a stand-in for fermionic B species, as path-integral QMC cannot simulate fermions due to the sign problem. While there is no direct mapping from hard-core bosons to fermions for local observables in three dimensions, we compared the hard-core and fermionic profiles for the single-species case and found excellent agreement. Based on this, we expect our results for the local density in the mixture to also be valid.

The two-component mixture is described by the Hamiltonian

$$H = -\sum_{\langle i\,j\rangle,\gamma} J_\gamma (a^\dagger_{i,\gamma} a_{j,\gamma} + \text{h.c.}) + \frac{U}{2}\sum_i n_{i,\rm A}(n_{i,\rm A}-1) + U_{\rm AB}\sum_i n_{i,\rm A} n_{i,\rm B} - \sum_{i,\gamma} \mu_{\gamma,i} n_{i,\gamma}. \qquad (4)$$

Here γ =A, B and $U_{\rm AB}$ is the interspecies on-site interaction which can be tuned to be repulsive or attractive. To study the effect of interspecies interactions we have performed simulations with $-40 < U_{\rm AB}/J_{\rm A} < 40$ with 10500 A atoms and 25000 B atoms. Previous studies have shown that at a given $T/J_{\rm A}$, the presence of attractive interactions enhances the conversion efficiency [31]. This corresponds to an enhancement of f_p measured at the same $T/J_{\rm A}$ for every $U_{\rm AB} < 0$. In Fig. 4 we show $f_p(T/J_{\rm A} = 0.2)$ and $f_p(T/J_{\rm A} = 10)$ as a function of $U_{\rm AB}/J_{\rm A}$ using filled squares and filled circles connected by a line, respectively. We normalize the values to f_p^0, the peak filling of A at $T/J_{\rm A} = 0.2$ in the absence of species B. As described above the peak filling gives an idea of the on-site densities in the distribution and normalizing to the zero-temperature, non-interacting case allows us to clearly identify any enhancement or depletion of the filling due to thermal or interaction effects. It is clear that attractive interactions lead to an enhancement of f_p if $T/J_{\rm A}$ is kept constant.

However, this simple analysis does not describe current experiments, since starting at the same initial temperature, T_i/T_F, T_F the Fermi temperature, leads to a final temperature $T_{\rm fin}/J_{\rm A}$ after adiabatic loading that depends on the sign and magnitude of $U_{\rm AB}$. In Fig. 4 (c) we show $T_{\rm fin}/J_{\rm A}$ for $U_{\rm AB}/J_{\rm A} = -40$, -10, 10, and 40 using solid, dash, dot-dash, and dot-dot-dash lines, respectively. From Fig. 4(c) it is clear that attractive interactions tend to cause more severe heating during the adiabatic loading. For the range of initial entropies considered in this work, this additional heating inhibits and counteracts the benefit gained by making the two species attract. In Fig. 4 (a) we show f_p as a function of $U_{\rm AB}/J_{\rm A}$ for T_i/T_F =0.1 and 0.3 using filled squares and filled triangles, respectively. Following adiabatic loading, both attractive and repulsive interactions destabilize the A species Mott insulator and reduce the peak filling.

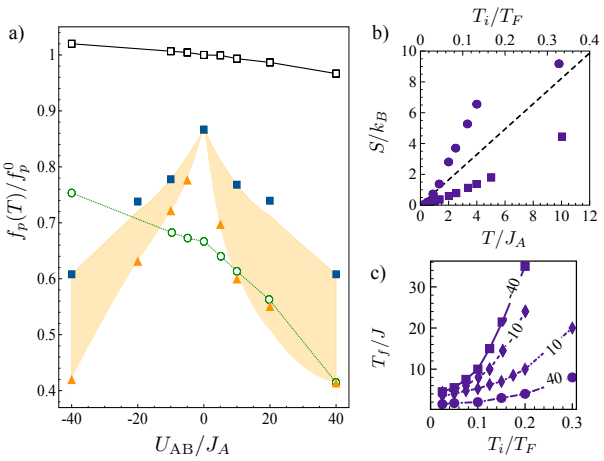

FIG. 4. (Color online) *Dependence of species A peak filling on* $U_{\rm AB}$. (a) Peak filling normalized to zero-temperature value, $f_p(T)/f_p^0$, vs. $U_{\rm AB}/J_{\rm A}$ at $T/J_{\rm A}$=0.2 (empty squares) and $T/J_{\rm A}$=10 (empty circles), ignoring the interaction dependence of the final temperature due to adiabatic loading. Accounting for interaction effects during loading at initial temperatures $T_i/T_F = 0.1$ (0.3) are given with filled squares (triangles). (b) The entropy of species A as a function of $T/J_{\rm A}$ is shown for $U_{\rm AB}/J_{\rm A} = 40$ and -40 using circles and squares, respectively. The dashed line is the entropy of non-interacting fermions in a harmonic trap, which we use as an estimate for S_i. (c) Final temperature vs. initial temperature for $U_{\rm AB}/J_{\rm A} = -40$, -10, 10, and 40 (solid, dash, dot-dash, and dot-dot-dash, respectively). We use a harmonic confinement of $\omega_r(\omega_z) = 2\pi \times 23(150)$ Hz

IV. EFFICIENCY OF FESHBACH MOLECULE PRODUCTION ON A SINGLE LATTICE SITE

The next stage in the production of molecules associates the two atoms on a lattice site into a weakly bound molecular state. The most common method of association is magnetoassociation, where a loosely bound Feshbach molecule is created by sweeping the magnetic field through a Feshbach resonance [11]. When this association process happens in a deep lattice, tunneling can be neglected. In this case a reasonable approximation is to replace each lattice site with a harmonic well. The validity of this approach for the molecular binding energy at $V_0 \approx 40E_A$ lattice depth was demonstrated in Ref. [20]. The formation efficiency of molecules has been shown to be mostly local in deep lattices. In this regime the atom-pair to molecule conversion is guaranteed to occur with essentially unit efficiency for particles in the ground band. This has been confirmed experimentally in a 3D lattice where nearly 100% conversion efficiency between Feshbach molecules and local pairs of K and Rb atoms was observed [36].

Within the harmonic oscillator approximation, there is an important subtlety regarding conversion of atoms in higher bands into molecules. If one of the atoms is in a higher band, the two-atom wavefunction consists of a superposition of states with an excitation in the relative coordinate and an excitation in the center of mass coordinate, with different weighting of these components in the case of mass or trapping frequency imbalance for the two species [21, 22]. The component corresponding to a relative excitation has a node at short distance, and so this channel will not become a molecule following magnetoassociation, and instead will remain as unbound atoms. In contrast, the center of mass excitation will be adiabatically converted to a molecule in a higher band following magnetoassociation. Thus, the conversion of excited band atoms to molecules in the first excited band is given by $P_{\rm M} = P_{\rm A}P_{\rm A\to M} + P_{\rm B}P_{\rm B\to M}$ where $P_{\rm M}$ is the probability of forming a molecule in the first excited band, $P_{\rm A(B)}$ is the probability of an atom of type A(B) occupying the first excited band after the loading procedure, and finally $P_{\rm A(B)\to M}$ is the probability of the pair with atom A(B) in the first excited band forming a molecule in the first

excited band. Since $P_{\mathrm{A(B)\to M}}$ is given by the relative weight of the center of mass excitation on the A and B species atoms, it depends on the mass and polarizability ratio and strength of interactions, and so in general it is highly species dependent. From this consideration minimizing band excitation of the preformed pairs is an important requirement for optimal molecule production in lattices.

In shallower lattices center of mass and relative coordinates couplings can enhance the conversion efficiency of excited band atoms to molecules. Moreover, tunneling processes can also convert atoms on different sites to molecules[23, 24]. However, since the tunneling rate decreases exponentially with lattice depth, the slow magnetoassociation ramp condition required to remain adiabatic and allow such non-local processes to happen is generally not satisfied in current experiments and to a good approximation the conversion at $V_0 \gtrsim 15E_A$ assumed to be mostly local.

In this section we outline how one can find $P_{\mathrm{A(B)}}$ and this method to KRb and LiCs molecules. While the experimental system is three-dimensional, for simplicity we restrict the discussion to a one-dimensional system. A framework for the three-dimensional problem has been developed in [25]. It should be noted that since the two species in the experiment experience different trapping potentials, the Hamiltonian does not separate into center of mass (CM) and relative coordinates, but contains a coupling between the two. Namely, the Hamiltonian is

$$\begin{aligned} H =& -\frac{\hbar^2}{2m_{\mathrm{B}}}\nabla_B^2 - \frac{\hbar^2}{2m_{\mathrm{A}}}\nabla_A^2 + \frac{1}{2}m_{\mathrm{B}}\omega_{\mathrm{B}}^2 x_{\mathrm{B}}^2 \\ &+ \frac{1}{2}m_{\mathrm{A}}\omega_{\mathrm{A}}^2 x_{\mathrm{A}}^2 + V_{\mathrm{int}}(r) \\ =& H_{\mathrm{CM}}(X) + H_{\mathrm{rel}}(x) + CXx, \end{aligned} \tag{5}$$

where

$$\begin{aligned} H_{\mathrm{CM}} &= -\frac{\hbar^2}{2M}\nabla_X^2 + \frac{1}{2}M\Omega^2 X^2\,, \\ H_{\mathrm{rel}} &= -\frac{\hbar^2}{2\mu}\nabla_x^2 + \frac{1}{2}\mu\omega^2 x^2 + V_{\mathrm{int}}(x), \end{aligned}$$

$M = m_{\mathrm{A}} + m_{\mathrm{B}}$, $\mu = m_{\mathrm{A}}m_{\mathrm{B}}/M$, and $V_{\mathrm{int}}(x)$ is a regularized contact pseudopotential parameterized by an interaction strength g. Here, Ω and ω are the CM and relative trapping frequencies, given by

$$\frac{\Omega}{\omega_{\mathrm{A}}} = \sqrt{\frac{1+\beta}{1+\alpha}}\,, \frac{\omega_{\mathrm{rel}}}{\omega_{\mathrm{A}}} = \sqrt{\frac{\alpha+\beta/\alpha}{1+\alpha}}\,,$$

and the CM/relative coupling is given by $\frac{C}{m_{\mathrm{A}}\omega_{\mathrm{A}}^2} = \frac{\alpha-\beta}{1+\alpha}$, where $\alpha = m_{\mathrm{B}}/m_{\mathrm{A}}$ and $\beta = m_{\mathrm{B}}\omega_{\mathrm{B}}^2/(m_{\mathrm{A}}\omega_{\mathrm{A}}^2)$.

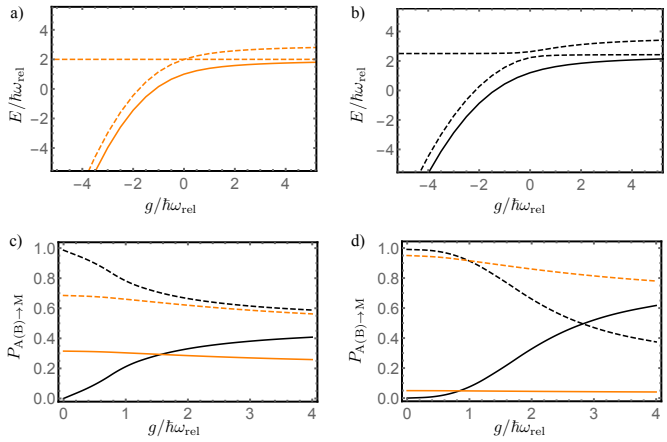

FIG. 5. (Color online) The conversion efficiency of higher band atoms to molecules. (a) The spectrum of the K and Rb using a single-site harmonic oscillator model. (a) The solid black (dashed orange) lines show the states with zero quanta (one quantum) of motional excitation with CM/relative coupling artificially set to zero. (b) Same as (a) but with CM/relative coupling included. (c) The solid (dashed) black line corresponds to the overlap between the eigenstate correlating to an excited molecule and an atom pair with an excited excited K (Rb). The orange lines are the same quantity without CM/relative coupling, showing strong CM/relative mixing for this system. (d) Same as (c) but for the LiCs system with Cs as species B, and $\omega_{\mathrm{Cs}}/\omega_{\mathrm{Li}} = 1.8$, showing a weaker degree of CM/relative coupling at small g.

In order to find the probabilities $P_{\mathrm{A}\to\mathrm{M}}$ and $P_{\mathrm{B}\to\mathrm{M}}$ we calculate the matrix elements of Hamiltonian (5) in the CM-rel basis, where the CM states $\phi_\eta(X)$ are harmonic oscillator functions, while the relative coordinate states are given by the fully non-perturbative solutions of Busch *et al.*[26], $\psi_\kappa(x)$. Figures 5(a) and (b) show the spectrum of a Rb/K atom pair with $\omega_{\mathrm{K}}/\omega_{\mathrm{Rb}} = 1.4$ as a function of interaction strength g in the absence and presence of the CM-rel coupling, respectively. In both panels the solid black (dashed orange) lines to show states with zero (one) total quanta of excitation. In the presence of CM/relative coupling (Panel (b)), the higher energy eigenstate correlating to a quantum of excitation tends to free atoms at large negative g, while the lower branch correlates to a molecule with a quantum of excitation. The deviation of the dashed lines from the $C = 0$ solutions depends on the experimental parameters, including the trapping frequencies and the atomic species.

As described above, the state with the CM excitation connects to the molecular state in the first excited band. Our task is to find how the excited atomic states connect to this state. To do so, we calculate overlaps between the molecular eigenstate (lower energy state in Fig. 5(b)) in the CM-rel basis and the atomic wave functions given by products of harmonic oscillator functions $\Psi(x_{\mathrm{A}}, x_{\mathrm{B}}) = \psi_{\mathrm{A}}^{\eta}(x_A)\psi_{\mathrm{B}}^{\kappa}(x_B)$, where η and κ represent band indices for the atomic wave functions. The square modulus of this quantity is precisely the probabil-

ity $P_{\mathrm{A(B)}\to\mathrm{M}}$. In figure 5(c) we show these overlaps as a function of interaction strength g for KRb. The dashed lines are the overlap between the excited molecular state and the atomic state $\psi^1_{\mathrm{A}}(x_{\mathrm{A}})\psi^0_{\mathrm{B}}(x_{\mathrm{B}})$, while the solid lines are the overlap with the atomic state with the B atom in the excited motional state, and black (orange) colors denote inclusion (exclusion) of the CM/relative coupling. Without CM/relative coupling, the relative weights onto the two atomic excitations is given roughly by the mass ratio, $\approx 1/3, 2/3$ in the case of KRb. However, strong CM/relative mixing in the KRb system means that the excited molecular state correlates to almost pure Rb excitation for weak interactions. Figure 5(d) shows a similar calculation for LiCs molecule. Here the dashed lines show the overlap between the molecular state in the first excited band and the Cs atom being excited, while the solid lines are the corresponding quantity with Li atom in the first excited band. The mass ratio for Li/Cs implies that the excited molecular state consists of almost pure Cs excitation even without CM/relative coupling. Additionally, the LiCs system displays a weaker coupling of the CM and relative coordinates.

V. STIRAP ADIABATICITY AND HIGHER-BAND TRANSFER

Feshbach molecules are converted into ground state molecules via a two-photon STIRAP sequence involving an intermediate electronically excited molecular state. As the STIRAP process must remove $\sim$ 100 THz of molecular energy, the difference of the wavevectors of the two photons involved in the STIRAP sequence, denoted by $\vec{k}_u$ and $\vec{k}_d$, can have significant variation on the lattice scale of a few microns. The resulting momentum transfer can excite the resulting ground state molecules to higher lattice bands. Here, we investigate the adiabaticity of the STIRAP procedure, as well as the rate of transfer of molecules to higher bands.

We consider a STIRAP process which couples the Feshbach molecule (FBM) ($|f\rangle$) and ground molecular (GSM) $|g\rangle$ states through an excited level ($|e\rangle$) [35]. We assume that these are the only states involved and neglect the population of other molecular levels or atomic scattering states during the STIRAP. To match current experiments, we study the case of vanishing single- and two-photon detunings. Using adiabatic perturbation theory [37, 38], as described in the appendix, we find that the momentum transfer following the process $|f\rangle \to |g\rangle$ has the same form as the case of large single-photon detuning, $\propto e^{i(\vec{k}_u-\vec{k}_d)\cdot\vec{r}}$. Typical STIRAP linewidths are $\sim$ 200kHz, significantly greater than the $\sim$ 20kHz spacing between bands, and so the band structure is fully unresolved. Thus, the relative population of molecules in the different bands following STIRAP are determined by ratios of Rabi frequencies in the basis of Wannier states with band index n. We use $w_n(\vec{r})$ and $\bar{w}_n(\vec{r})$ to denote the Wannier states for FBM and GSM, respectively. For FBM in the lowest band, the relative population of GSM in the first excited band along the direction ξ can thus be estimated by

$$\left|\frac{\langle\bar{w}_1|e^{ik_\xi\xi}|w_0\rangle}{\langle\bar{w}_0|e^{ik_\xi\xi}|w_0\rangle}\right|^2 \approx \frac{2(k_\xi a)^2\tilde{\alpha}}{\pi^2(1+\tilde{\alpha})^2\sqrt{V/E_R}}, \qquad (6)$$

where we have used a harmonic approximation for the Wannier functions, with $k_\xi \equiv (\vec{k}_u - \vec{k}_d)\cdot\vec{\xi}$ the momentum transfer along direction ξ, a the lattice spacing, $\tilde{\alpha}$ the polarizability ratio of the GSM to the FBM, V the lattice depth for the FBM, and E_R the molecular recoil energy. For the parameters of the JILA experiment [1], $a = 532$ nm, $k_u = 2\pi/(968\text{ nm})$ and $k_d = 2\pi/(689\text{ nm})$ co-propagating at a 45° angle with respect to the x and y lattice axes, and $\tilde{\alpha} \approx 0.9$, we find the total population in the first excited bands to be $\sim 1\%$. In general, our results indicate that for experiments in the Lamb-Dicke regime $k_\xi a/(V/E_R)^{1/4} \ll 1$, STIRAP does not induce appreciable population transfer to excited bands.

In conclusion, we studied the combined effects of interspecies interactions, temperature, and adiabatic loading on the successful preparation of a low entropy gas of polar molecules. We have shown that interspecies interactions have have a significant effect on the final temperature of the lattice gas following adiabatic loading, which in turn can lead to the depletion of the peak filling of the bosonic species and a lower efficiency of molecule formation. Based on our results, molecule formation efficiency is greatest when the lattice loading is performed with a non-interacting mixture. This does not agree with previous studies, which do not treat the adiabatic loading procedure and find that attractive interspecies interactions enhance the on-site densities. We observe that the latter statement only holds if the gas is initially prepared at significantly lower temperatures than the ones currently reached in experiments: for the parameters considered in this work around $T/T_F \lesssim 0.05$, which translates in final temperature after loading is $T_{\mathrm{fin}}/J_{\mathrm{A}} \lesssim 5$

Acknowledgments We would like thank M. Gärttner and B. Capogrosso-Sansone for useful discussions. This work was supported by the NSF (PIF-1211914 and PFC-1125844), AFOSR, AFOSR-MURI, NIST and ARO individual investigator awards. MLW thanks the NRC for support. Part of the computing for this project was performed at the OU Supercomputing Center for Education & Research (OSCER) at the University of Oklahoma (OU). This work also utilized the Janus supercomputer, which is supported by the National Science Foundation (award number CNS-0821794) and the University of Colorado Boulder. The Janus supercomputer is a joint effort of the University of Colorado Boulder, the University of Colorado Denver and the National Center for Atmospheric Research.

Appendix A: Appendix: Adiabaticity of the STIRAP procedure

Stimulated Raman adiabatic passage (STIRAP) is a commonly used procedure to convert Feshbach molecules (FBM), formed following a magneto- or photo-assocation step, to ground state molecules (GSM). The STIRAP sequence couples the FBM ($|f\rangle$) and the GSM ($|g\rangle$) states through an intermediate excited molecular state, $|e\rangle$. In the most commonly employed "counter-intuitive" pulse sequence, the time-dependent Hamiltonian describing the system is

$$H = \Delta|e\rangle\langle e| + \Omega t/\tau \left(e^{i\vec{k}_u\cdot\vec{r}}|e\rangle\langle f| + \text{h.c.}\right) + \Omega(1-t/\tau)\left(e^{i\vec{k}_d\cdot\vec{r}}|e\rangle\langle g| + \text{h.c.}\right), \quad \text{(A1)}$$

where $\vec{k}_u$ and $\vec{k}_d$ are the wave vectors of the two photons in the STIRAP sequence and Δ is the single-photon detuning. While for large Δ the intermediate $|e\rangle$ can be adiabatically eliminated in favor of a direct two-photon coupling $\propto \frac{\Omega^2}{\Delta}e^{i(\vec{k}_u-\vec{k}_d)\cdot\vec{r}}$ from $|f\rangle$ to $|g\rangle$ and standard Landau-Zener estimates can be used, current experiments use $\Delta = 0$, where the degree of adiabaticity and momentum transfer are less clear. We therefore treat $\Delta = 0$, where current experiments operate, using adiabatic perturbation theory (APT) [37, 38]. In this approach, we expand the wavefunction as $|\psi(t)\rangle = \sum_n \alpha_n(t)e^{-ia\theta_n(\lambda)}|\phi_n(t)\rangle$, where $|\phi_n(t)\rangle$ are the adiabatic basis states satisfying $H(t)|\phi_n(t)\rangle = E_n(t)|\phi_n(t)\rangle$, $a = \Omega\tau$ is the adiabatic parameter, $\lambda = t/\tau$, and $\theta_n(\lambda) = \int^\lambda d\lambda' E_n(\lambda')/\Omega$ is the dimensionless geometric phase. Expanding the solution of the differential equations satisfied by the $\{\alpha_n\}$ to lowest order in τ^{-1}, we find analytic expressions for $\alpha_{f,e,g}(\lambda)$,

$$\alpha_f(\lambda) = \frac{1-\lambda}{\sqrt{b}} + \frac{\lambda\sin(a\theta_1(\lambda))}{ab^2}, \quad \text{(A2)}$$

$$\alpha_e(\lambda) = -\frac{i}{a}\left(1 - \frac{\cos(a\theta_1(\lambda))}{b}\right), \quad \text{(A3)}$$

$$\alpha_g(\lambda) = e^{i(\vec{k}_u-\vec{k}_d)\cdot\vec{r}} \times \left[-\frac{\lambda}{\sqrt{b}} + \frac{(1-\lambda)\sin(a\theta_1(\lambda))}{ab^2}\right], \quad \text{(A4)}$$

where $b = 1 + 2\lambda(\lambda-1)$. For completeness, we note that $\theta_1(\lambda)$ can be determined analytically to be

$$\theta_1(t) = \frac{a}{4}\left[1 + (2\lambda-1)\sqrt{b} + \frac{1}{\sqrt{2}}\left(\text{arcsinh}(1) - \text{arcsinh}(1-2\lambda)\right)\right], \quad \text{(A5)}$$

and so the above expressions provide fully analytic estimates for the degree of adiabaticity. The results of a numerical simulation of the STIRAP process for reasonable experimental parameters $\Omega = 5$MHz, $\tau = 6\mu$s are shown in Fig. 6 (yellow), together with the residual error of the first-order expressions Eqs. (A2)-(A4) (blue).

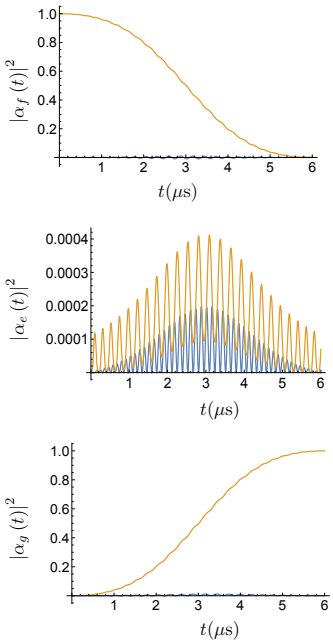

FIG. 6. (Color online) Populations of the Feshbach molecule, excited, and ground states during the STIRAP sequence with Ω =5MHz and $\tau = 6\mu$s (yellow), together with the residual of the first-order expressions Eqs. (A2)-(A4) (blue).

[1] Steven A. Moses, Jacob P. Covey, Matthew T. Miecnikowski, Bo Yan, Bryce Gadway, Jun Ye, and Deborah S. Jin, arXiv:1507.02377.

[2] L. D. Carr, D. Demille, R. V. Krems, and J. Ye, New J. Phys. **11**, 055049 (2009).

[3] M. A. Baranov, M. Dalmonte, G. Pupillo, and P. Zoller, Chemical Reviews **112**, 5012 (2012).

[4] M. L. Wall, K. R. A. Hazzard, and A. M. Rey, Chapter in "From atomic to mesoscale: The Role of Quantum Coherence in Systems of Various Complexities" ed. S. Malinovskaya and I. Novikova,World Scientific (2015) arXiv:1406.4758.

[5] Norman Y. Yao, Chris R. Laumann, Sarang Gopalakrishnan, Michael Knap, Markus Muller, Eugene A. Demler, and Mikhail D. Lukin, Phys. Rev. Lett. 113, 243002 (2014).

[6] Sergey V. Syzranov, Michael L. Wall, Victor Gurarie, and Ana Maria Rey, Nature Communications **5**, 5391 (2014).

[7] D. Peter, N. Y. Yao, N. Lang, S. D. Huber, M. D. Lukin, and H. P. Büchler, Phys. Rev. A **91**, 053617 (2015).

[8] B. Yan, S. A. Moses, B. Gadway, J. P. Covey, K. R. A. Hazzard, A. M. Rey, D. S. Jin, and J. Ye, Nature **501**, 521 (2013).

[9] B. Zhu, B. Gadway, M. Foss-Feig, J. Schachenmayer, M. L. Wall, K. R. A. Hazzard, B. Yan, S. A. Moses, J. P. Covey, D. S. Jin, J. Ye, M. Holland, and A. M. Rey, Phys. Rev. Lett. **112**, 070404 (2014).

[10] K. R. A. Hazzard, B. Gadway, M. Foss-Feig, B. Yan, S. A. Moses, J. P. Covey, N. Y. Yao, M. D. Lukin, J. Ye, D. S. Jin, and A. M. Rey, Phys. Rev. Lett. **113**, 195302 (2014).

[11] K.-K. Ni, S. Ospelkaus, M. H. G. de Miranda, A. Pe'er, B. Neyenhuis, J. J. Zirbel, S. Kotochigova, P. S. Julienne, D. S. Jin, and J. Ye, Science **322**, 231 (2008).

[12] H. Cho, D. McCarron, D. L. Jenkin, M. P. Köppinger, and S. L. Cornish, European Physical Journal D 1 (2011), 10.1140/epjd/e2011-10716-1.

[13] M. Debatin, T. Takekoshi, R. Rameshan, L. Reichsöllner, F. Ferlaino, R. Grimm, R. Vexiau, N. Bouloufa, O. Dulieu, and H.-C. Nagerl, Phys. Chem. Chem. Phys. **13**, 18926 (2011).

[14] T. Takekoshi, M. Debatin, R. Rameshan, F. Ferlaino, R. Grimm, H.-C. Nägerl, C. R. Le Sueur, J. M. Hutson, P. S. Julienne, S. Kotochigova, and E. Tiemann, Phys. Rev. A **85**, 032506 (2012).

[15] T. Takekoshi, L. Reichsöllner, A. Schindewolf, J. M. Hutson, C. R. Le Sueur, O. Dulieu, F. Ferlaino, R. Grimm, and H.-C. Nägerl, Phys. Rev. Lett. **113**, 205301 (2014) .

[16] C.-H. Wu, J. W. Park, P. Ahmadi, S. Will, and M. W. Zwierlein, Phys. Rev. Lett. **109**, 085301 (2012).

[17] M.-S. Heo, T. T. Wang, C. A. Christensen, T. M. Rvachov, D. A. Cotta, J.-H. Choi, Y.-R. Lee, and W. Ketterle, Phys. Rev. A **86**, 021602 (2012).

[18] S. Dutta, J. Lorenz, A. Altaf, D. S. Elliott, and Y. P. Chen, Phys. Rev. A **89**, 020702 (2014).

[19] C. Ospelkaus, S. Ospelkaus, L. Humbert, P. Ernst, K. Sengstock, and K. Bongs, Phys. Rev. Lett. **97**, 120402 (2006).

[20] F. Deuretzbacher, K. Plassmeier, D. Pfannkuche, F. Werner, C. Ospelkaus, S. Ospelkaus, K. Sengstock, and K. Bongs, Phys. Rev. A. **77**, 032726 (2008).

[21] J. F. Bertelsen and K. Mølmer, Phys. Rev. A **76**, 043615 (2007).

[22] K. Jachymski, Z. Idziaszek, and T. Calarco, Phys. Rev. A **87**, 042701 (2013).

[23] J. von Stecher, V. Gurarie, L. Radzihovsky, and A. M. Rey, Phys. Rev. Lett. **106**, 235301 (2011)

[24] M. L. Wall and L. D. Carr Phys. Rev. Lett. **109**, 055302 (2012); M. L. Wall and L. D. Carr, Phys. Rev. A **87**, 033601 (2013).

[25] J. F. Bertelsen and K. Mølmer, Phys. Rev. A 76, 043615 (2007)

[26] Thomas Busch, Berthold-Georg Englert, Kazimierz Rzaz?ewski ,and Martin Wilkens, Foundations of Physics 28, 549 (1998).

[27] J. W. Park, S. A. Will, and M. W. Zeierlein, Phys. Rev. Lett. **114**, 205302 (2015).

[28] G. Quéméner and P. S. Julienne, Chemical Reviews **112**, 4949 (2012).

[29] N. V. Prokof'ev, B. V. Svistunov, and I. S. Tupitsyn, Phys. Lett. A **238**, 253 (1998); Sov. Phys. JETP **87**, 310 (1998).

[30] B. Damski, L. Santos, E. Tiemann, M. Lewenstein, S. Kotochigova, P. Julienne, and P. Zoller, Phys. Rev. Lett. **90**, 110401 (2003).

[31] J. K. Freericks, M. M. Maśka, Anzi Hu, Thomas M. Hanna, C. J. Williams, P. S. Julienne, and R. Lemański, Phys. Rev. A **81**, 011605(R), (2010).

[32] D. Jaksch, V. Venturi, J.I. Cirac, C.J. Williams, and P. Zoller, Phys. Rev. Lett. **89**, 040402 (2002).

[33] L. Pollet, C. Kollath, U. Schollwoeck, and M. Troyer, Phys. Rev. A **77**, 023608 (2008).

[34] L. Pollet, C. Kollath, K. Van Houcke, and M. Troyer, New J. Phys. **10** 065001 (2008).

[35] S. Ospelkaus, A. Pe'er, K. K. Ni, J. J. Zirbel, B. Neyenhuis, S. Kotochigova, P. S. Julienne, J. Ye, and D. S. Jin, Nature Physics, 4, 622 - 626 (2008).

[36] A. Chotia, B. Neyenhuis, S. A. Moses, B. Yan, J. P. Covey, Michael Foss-Feig, A. M. Rey, D. S. Jin, and J. Ye, Phys. Rev. Lett. **108**, 1 (2012)

[37] A. Polkovnikov, Phys. Rev. B **72**, 161201(R) (2005).

[38] G. Rigolin, G. Ortiz, and V. H. Ponce, Phys. Rev. A **78**, 052508 (2008).